

## Experimental Analysis on 3d Printed Onyx Specimens with Honeycomb Infill Structure

Raghuram Pipalla<sup>1\*</sup>, Jens Schuster<sup>2</sup> and Yousuf Pasha Shaik<sup>3</sup>

<sup>1</sup>Student at University of Applied Sciences Kaiserslautern, Germany.

<sup>2</sup>Professor at University of Applied Sciences Kaiserslautern, Germany.

<sup>3</sup>Research Associate at University of Applied Sciences Kaiserslautern, Germany.

### \*Correspondence:

Raghuram Pipalla, Student at University of Applied Sciences Kaiserslautern, Germany.

Received: 01 August 2021; Accepted: 25 August 2021

**Citation:** Pipalla R, Schuster J, Shaik YP. Experimental Analysis on 3d Printed Onyx Specimens with Honeycomb Infill Structure. J Adv Mater Sci Eng. 2021; 1(1): 1-10.

### ABSTRACT

There is a demand for the development of products in a shorter time that resulted in the introduction of 3D printing which is also termed as “Additive Manufacturing” (AM). This technology has many advantages such as cost-effectiveness, less manufacturing time and elimination of post-processing costs. Intensive research is being carried out on cellular structures manufactured using additive manufacturing technologies. Cellular structures have many applications in various areas. When compared to solid structures, these cellular structures possess high strength to weight ratio, good energy absorption characteristics, good thermal and acoustic insulation properties. They are used for aerospace, medical and engineering products. There are many additive manufacturing technologies whereas fused deposition modelling (FDM) is the most versatile one. This research consists of the analysis of hexagonal honeycomb structure by creating honeycomb structures of different dimensions in SolidWorks and manufacturing of those structures by using the FDM additive manufacturing process. These structures were designed by varying the internal hexagon's wall thickness and side length. After printing these structures were subjected to Mechanical testings like tensile, compression, three-point bending, impact and thermal testing like heat deflection temperature tests. The three-point bending test was simulated numerically and compared with the experimental results. This study is finally validated by comparing experimental and simulation results, which were in agreement with each other. Experimental results show that the low-weight specimen exhibited good mechanical and thermal properties with a lesser printing time compared to the remaining specimens. The specimens with different hexagonal cell dimensions were introduced and discussed.

### Keywords

Hexagonal cellular structure, Onyx, Mechanical properties, Thermal properties, Side length, Wall thickness.

### Introduction

Additive manufacturing is an additive fabrication process to prepare a 3D object. The three-dimensional part is produced by combining layers of 2-D cross-sectional slices of materials one over another [1,7]. During this process, there is no external tool usage and human intervention. This technology is developed in the mid-1980s [2]. During this period, 3D printing is termed “Rapid Prototyping” (RP). The very first patent application for RP technology was filed by Dr. Kodama in 1985. Chuck Hull, of 3D

Systems Corporation, manufactured the first usable 3D printer [3]. Later in the 90's, Selective Laser Sintering (SLS) technology was synthesized by Dr. Deckard at the University of Texas during the commencement of a project being done by the Defense Advanced Research Projects Agency [4]. In the 20<sup>th</sup> century, 3D printers were very expensive and were used to print a few numbers of products. Most of the printers were owned by scientists and electronics groupies for research and display. However, advancements in the area of 3D printing (3DP) has allowed for the design of products to no longer be limited by complex shapes or colors. Varieties of 3D printing technologies have been developed with different functions. According to ASTM Standard F2792 [5], ASTM catalogued 3D printing technologies into seven groups, including the binder jetting [6], directed energy deposition [7], material extrusion [8], material

jetting [9], powder bed fusion [10], sheet lamination [11] and vat photopolymerization [12]. Nowadays, 3D printing technologies are no longer limited to prototyping usage but are increasingly also being used for making a variety of products [13]. Due to the wide range of availability of materials FDM can produce functional parts for various industrial applications including aerospace, automobile and medical sectors. BMW and Bentley Motors use the FDM process to produce their automobile components which reduces their build time and cost up to 50 percent compare to the conventional CNC machining process. The 3D printer used in this research is Mark Forged Mark Two which works on the principle of continuous filament fabrication (CFF) [14] and ONYX material used to make objects. Onyx is stronger, harder and more resistant to heat than other plastic 3D printing materials [15].

## Background

Fused Deposition Modelling (FDM) was introduced and commercialized by Stratasys, Minnesota, USA in 1991. The need for minimizing the expensive build materials, fabrication time, energy consumption motivated researchers towards designing cellular structures since a key advantage offered by such structures is a high strength accompanied by a relatively low mass. However, due to their complexity, it is often difficult to manufacture them using conventional manufacturing processes. In this regard, advances in AM and CAD systems have allowed for the creation of complex geometries with a relatively high level of precision. AM can produce structures without any broken cells and geometrical defects [16].

Among the available processes, the material extrusion principle, also referred to as Fused Deposition Modelling (FDM) is considered as the most widely used technology among all types of 3DP technology around the globe because of its cost convenience and simplicity [17].

The evolution of FDM begins with thermoplastic resin printing, which is also known as fused filament fabrication (FFF). The FFF printed items show poor mechanical properties, hence are more commonly used as prototype products or toys [18].

Therefore, to widen the application of 3D printed FDM technology for designing high-performance composites, continuous fiber-reinforced composite is of a pressing need. The technology available in the market with this feature is known as continuous filament fabrication (CFF) [14].

Several authors [19-26] have reported on the use of 3D printed structures as energy absorption solutions. Although the majority of the referred studies [19-21, 23-25] resorted to experimental quasi-static compression tests to evaluate the energy absorption capabilities.

Hexagonal infill structure specimens (ASTM D790-10) exhibited the best mechanical performance in terms of specific flexural modulus and strength. Square infill structure specimens (ASTM D638-14) presented as expected the best mechanical performance

in terms of tensile modulus and strength [27].

Onyx-glass fiber Specimens with higher infill densities yielded under higher ultimate tensile load [28].

## Motivation of the work

Lightweight high-performance materials are in demand for engineering applications such as in the automotive and aerospace industries. The weight reduction is generally achieved by using cellular materials. There are many advantages if solid structures are replaced with cellular structures. Nowadays cellular structure application is increasing in engineering applications to reduce the weight and to get good mechanical and thermal properties. From the previous experiments, it was observed that the hexagonal cell structure gives more desirable properties [26], but dimensions for the optimized hexagonal structure are not discussed. In order to determine the optimized properties, various tests were performed on 3D printed specimens with hexagonal infill cellular structures of different dimensions were printed on Mark Forged Mark Two with onyx material.

## Objectives

The project aims to determine an optimized cellular structure for the production of any type of open-source designs in the field of automotive and aerospace industries by varying the hexagonal cellular structure side length and wall thickness with constant infill percentage.

## Methodology

### Fused Deposition Modelling

The FDM process allows manufacturing the parts or prototypes by extruding material like ABS, PLA, Onyx and Nylon, etc. through a nozzle that traverses in X and Y to create each two-dimensional layer. Instructions for the nozzle directions are given by STL file, which consists of G-Code. As each layer is extruded, it bonds to the previous layer and solidifies. The platform is then lowered relative to the nozzle and the next slice of the part is deposited on top of the previous slice. A second nozzle can also be used to extrude a different material to build up support structures for the part where needed or to manufacture composites. Once the part is completed, the support structures are removed. Figure 1, shows a schematic diagram of FDM-Process [25], where blue color indicates the model material and red color depicts the support material.

### Equipment and Material

The Mark Forged Mark Two desktop 3D printer was developed to overcome the strength limitations inherent in many 3D printing materials as shown in Figure 2. The Mark Forged Mark Two printer is the world's first 3D printer to print composite materials. Now functional parts, tools and devices can be printed with a much better strength-to-weight ratio. The continuous fiber printing technology is called Continuous Filament Fabrication (CFF). Continuous fiber fabrication method using traditional 3D printers with modified printing head [14]. Unlike chopped fiber-reinforced composites it has two separate nozzles for feeding two different materials. Printing with single material is also possible with Mark

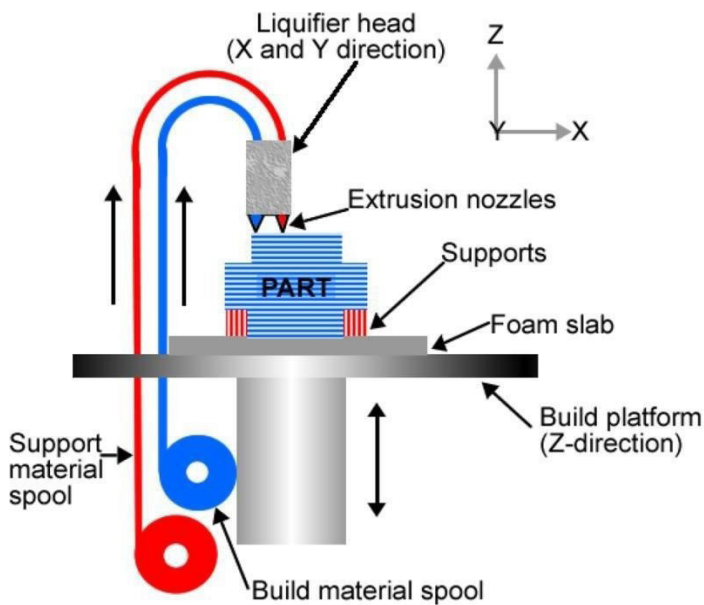


Figure 1: Basic method of FDM technology [25].

Forged Mark Two. The input for the 3D printer was 3D CAD models in STL format. STL file controls the nozzle movements [29]. When the extruder temperature raises then the material which is passing through this extruder reaches to glass transition temperature then depositing material onto the printing bed layer by layer. The temperature of the nozzle is selected based on the thermal properties of the thermoplastic polymer. As soon as the material is deposited and reached the printing bed, it solidifies quickly and sticks to the previous layer. The printing head as shown in Figure 3, is designed to move in 2D motions i.e., X-Y directions and is responsible to design each layer according to the trajectory of the 3D CAD model transferred by slicing software. The third movement along the Z direction to a distance equal to the layer thickness is accomplished by the building platform after each layer is made, which is continued until the structure is completed.

Onyx is a material based and extremely rigid nylon in combination with micro-carbon fibers. It is stronger, harder and more resistant to heat than commercial plastic 3D printing materials. It is the ideal material to produce parts that require a good look in compliance with industry requirements. The material provides toughness of nylon with the added stiffness of fiber-reinforced plastic, heat resistance up to 145° C and high resistance to adverse conditions [15]. The final product does not require any post-processing because its smooth and matte surface does not look like a piece that was printed on a 3D printer. Onyx can be used alone or reinforced with Kevlar, glass or carbon fibers. The parts reinforced by these fibers extend beyond the boundaries of the normally 3D extruded plastic. According to Mark Forged, parts printed with Onyx are 30% stronger and stiffer than similar parts made in other 3D printers and the properties are shown in Table 1. All products printed with Onyx are ready for use right after printing.

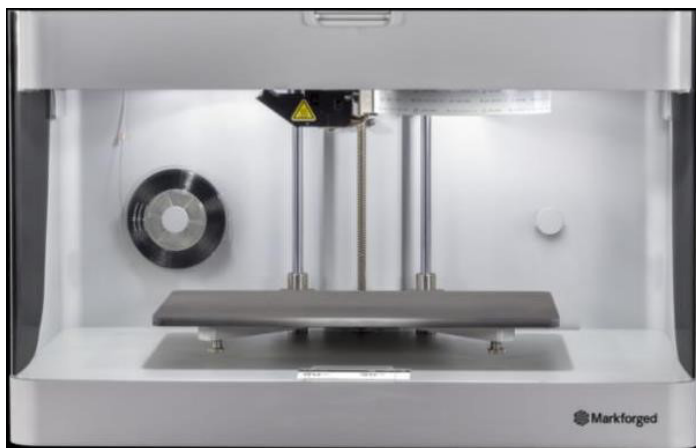


Figure 2: Mark forged mark two.

Table 1: Properties of Onyx.

Technical specifications of Onyx			
Density	1180 kg/m <sup>3</sup>	Flexural modulus	3.6 GPa
Specific heat capacity	2050 J/(kg K)	Tensile modulus	1.4 GPa
Heat deflection temperature	145°C	Flexural strength	81 MPa
Poisson's ratio	0.3	Tensile strength	36 MPa
Thermal conductivity	0.2256 W/(m K)	Thermal expansion coefficient	72 × 10 <sup>-6</sup> W/(m K)

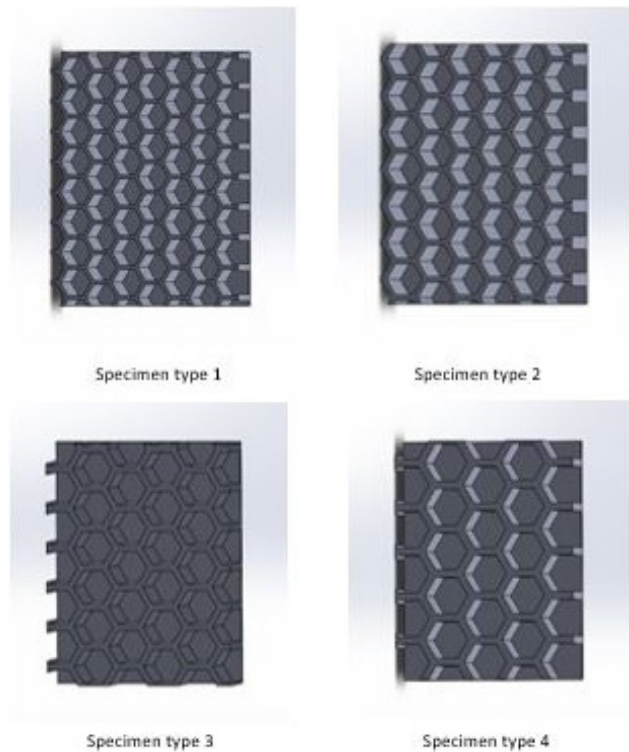


Figure 3: Printing head.

3D specimens were designed with the CAD program SolidWorks. The methodology for generating honeycomb structures consists of two phases. Phase 1 is related to creating a rectangular cuboid, while face 2 facilitates the creation of a honeycomb structure on the generated part in phase 1. The parts were designed in the solid works with the standard dimensions and the infill structure dimensions for all test specimens are shown in Table 2 and the infill structure with varying cell dimensions are shown in Figure 4, The designed specimens in SolidWorks have to be saved as an STL-file. STL format has been followed as the standard input for the 3D printing industry.

**Table 2:** Hexagonal cell dimensions.

Specimen number	Side length [mm]	Wall thickness [mm]
1	2.4	0.6
2	2.8	0.8
3	3.2	1.0
4	3.6	1.2



**Figure 4:** Infill structure with varying cell dimensions.

Eiger is a slicing software and very easy to use. Components can be quickly optimized with the right settings and fiber orientations to optimally design the component for different applications. The component created on the CAD- program as an STL file can easily load into the cloud-based Eiger Software via the browser (e.g., Google Chrome). STL files can be managed and catalogued. After uploading the CAD model in STL file format, printing parameters can select and change according to the requirement. Some of those parameters are wall thickness, layer height, fill density, infill structure, supports and print orientation, etc. If printing with supports turned on, the support structure will be generated automatically. The animated preview mode allows users to inspect all aspects of the print orientation before execution. The software reads the G-code and displays layer by layer how the model will be constructed.

## Experiments

### Finite element modelling (FE)

The FE analysis of the three-point bending test was conducted using SolidWorks Simulation, shown in Figure 5. The specimen was placed between two lower fixed supports and upper support that moves until maximum stress and minimum stress at maximum

deflection (f2) and minimum deflection (f1) respectively. The support span was taken as 64 mm. The point chosen for analysis has the same coordinates in all simulated specimens. The meshes of the supports and honeycombs were made automatically by defining the approximate global size. The simulation was done by fixing the fixtures at the bottom and sides of the supports and applying prescribed displacement in the middle of the specimen at the top [30].

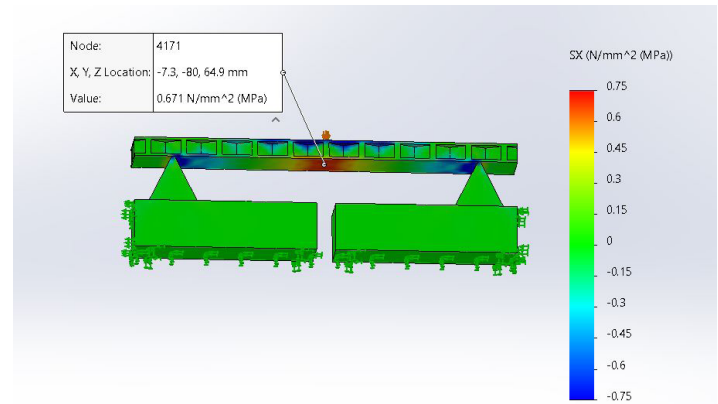


**Figure 5:** Simulation for 3 Point bending test.

Determination of the Equivalent stiffness equation between 0.05 and 0.25% in MPa.

$$\text{Equivalent stiffness equation } (E) = \frac{\sigma_2 - \sigma_1}{\epsilon_2 - \epsilon_1} \quad (1)$$

$$\text{Outer fiber strain } (\epsilon_b) = \frac{6hf}{lv^2} * 100\% \quad (2)$$

$$\text{span-to-thickness ratio } (lv) = (16 \pm 1)h \quad (3)$$

To calculate the stress in equivalent stiffness equation (E) firstly calculate the outer fiber strain at 0.05 and 0.25% displacement. f1 and f2 are obtained by the outer fiber strain formula. furthermore, by using these values in simulation  $\sigma_1$ ,  $\sigma_2$  values are determined and  $\epsilon_1$ ,  $\epsilon_2$  is 0.0005 and 0.0025 respectively.

For outer fiber strain calculation, the following parameters are considered.

Length l = 80 mm, Width b = 10 mm, Thickness h = 4 mm and Span to thickness ratio lv = 64 mm

From the equation (2), f1 = 0.0853 mm and f2 = 0.426 mm were determined and the values depicted in Table 3.

### Tensile tests

The tensile tests were performed according to DIN EN ISO 527 with dog-boned samples. The test samples were precisely held by top and bottom grips attached to the tensile or universal testing machine. Then, enter the load position '0'. During the tension test, the grips were moved apart at a constant test speed of 20 mm/min to pull and stretch the specimen. The force on the specimen and its displacement were continuously monitored and the stress-strain curve was plotted until failure. Tensile tests measure the force

required to break a plastic sample specimen  $\sigma_B$ , tensile modulus  $E_p$ , yield strength  $\sigma_y$  and yield strain  $\epsilon_y$ . Specimens were placed in the grips of the universal tester at a specified grip separation of 115 mm and pulled until failure as shown in Figure 6. A video-extensometer is used to determine the strain at break  $\epsilon_B$ , tensile modulus in begin  $\sigma_{low}$  and at the end  $\sigma_{high}$ .

### Heat deflection temperature tests (HDT)

The HDT/Vicat A tests were carried out according to DIN EN ISO 306. The test device is shown in Figure 7, consists of a bath with an option to mount measuring heads. A built-in thermostat controls the bath temperature. The thermostat ensures a constant increase of the temperature with the standardized gradient of 120 K/h over the entire test sequence. The heat deflection temperature is defined as the temperature at which a standard test bar deflects under a specified load. It is used to compare the mechanical performance of polymers at elevated temperatures. The bars were placed under the deflection measuring device. Load 306 g is placed on each specimen. The specimens are then lowered into a silicon oil bath where the temperature is raised.

In principle, it is a three-point-bending test in flat-wise configuration and uses specimens with dimensions 80 x 10 x 4 mm.

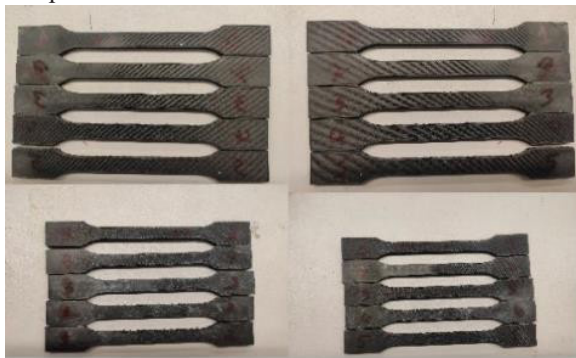


Figure 6 (a): Specimens before testing.



Figure 6 (b): Specimen after testing.

### Compression tests

Compressive properties describe the behaviour of a material when it is subjected to a compressive load according to the standard DIN EN ISO 604. Compressive strength  $\sigma_M$  and modulus  $E_c$ , are two common values generated by the test. Specimens prepared with the dimensions of 40 x 30 x 10 mm. The specimen is placed between compressive plates parallel to the surface is shown in

Figure 8. The specimen is then compressed at a uniform rate of 10 mm/min. The load applied on each specimen is 15000 N and the maximum bearing load was recorded along with stress-strain data, here compressive stress  $\sigma_B$ , strain  $\epsilon_B$  at break point values were obtained. An extensometer attached to the front of the fixture is used to determine the compression modulus in begin  $\sigma_{low}$  and at the end  $\sigma_{high}$ .

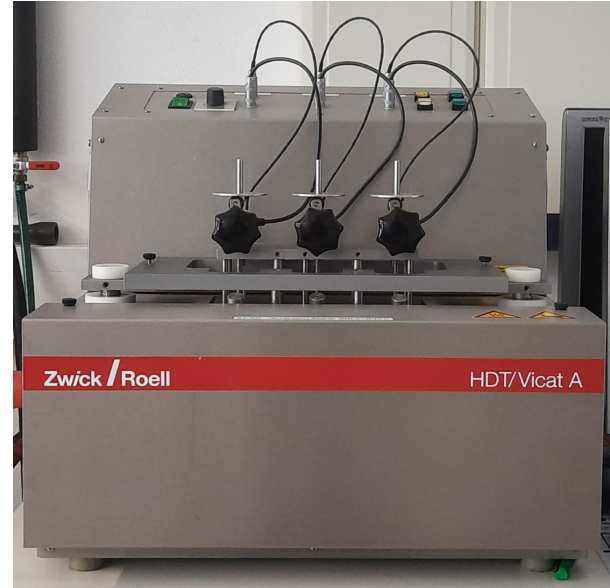


Figure 7: HDT machine.

### Three-point flexural tests

The flexural test according to DIN EN ISO 178 measures the force required to bend a beam under three-point loading conditions. Since the physical properties of many materials (especially thermoplastics) can vary depending on ambient temperature, it is sometimes appropriate to test materials at temperatures that simulate the intended end-use environment. The specimen lies on a support span and the load is applied to the centre by the loading nose producing three-point bending at a test speed of 10 mm/min. Flexural modulus in begin  $\sigma_{low}$ , and at end  $\sigma_{high}$  measured. A variety of specimen shapes can be used for this test, but the most used specimen size for ISO is 80 x 10 x 4 mm. From this test the flexural modulus  $E_p$ , flexural stress at standard deviation  $\sigma_{fc}$  values were determined.

### Impact tests

Charpy Impact tests were performed according to DIN EN ISO 179. It is a single-point test that measures the material's resistance to an impact from a swinging pendulum with a velocity of 2.9 m/s, the weight of the hammer is 0.9510 kg and impact energy 3.99 joules. The charpy impact is defined as the energy needed to initiate fracture and continues the fracture until the specimen is broken. The specimen is mounted horizontally and supported unclamped at both ends. The hammer is released and allowed to strike through the specimen is shown in Figure 9. The impact strength KJ/m<sup>2</sup> value was obtained. Unnotched Specimens with the dimensions 80 x 10 x 4 mm.

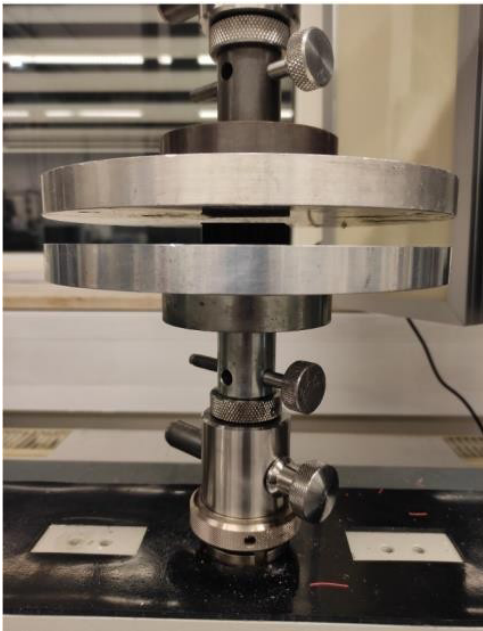


Figure 8: Compression test.

### Results and Discussion

Experimental and numerical modelling of three-point bending tests were conducted to evaluate the mechanical properties of the structures. For the Onyx samples, a very good correlation between numerical and experimental results are found and shown in Figure 10. The flexural modulus decreases from specimen type 1 to 3 because stress is very low. But side length 3.6 mm and wall thickness 1.2 mm specimen type has higher flexural modulus because the stress was high due to high wall thickness, and the results are shown in Table 3.

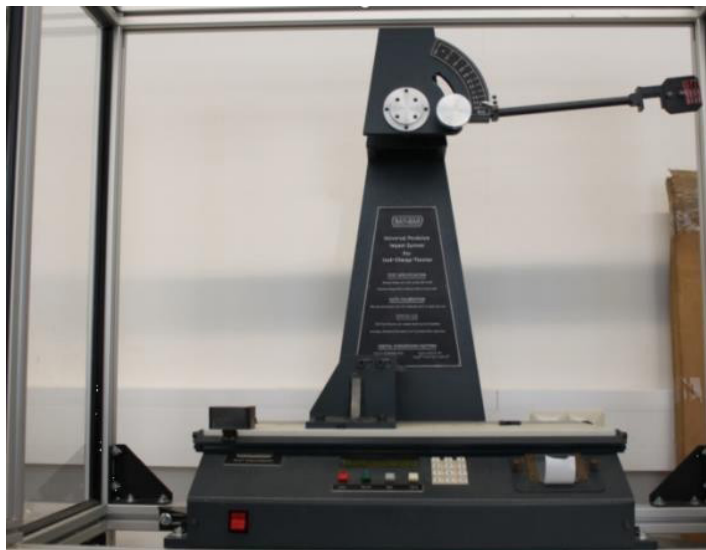


Figure 9: Impact machine.

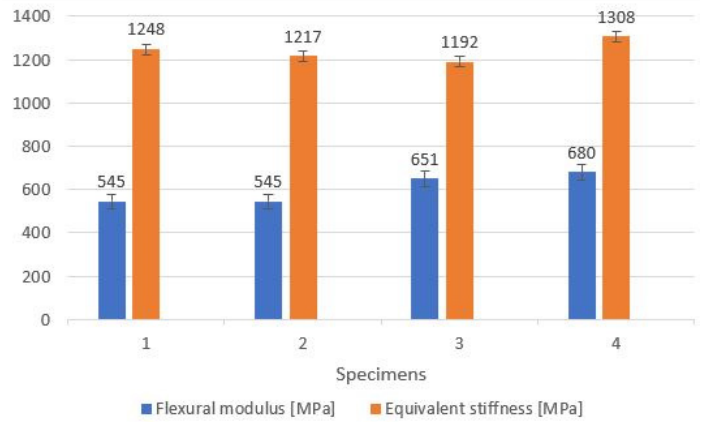


Figure 10: Comparison between experimental tests and numerical simulation for three-point bending test.

Figure 11, shows a plot of stress vs strain for all tensile test specimens. The obtained results are shown in Table 4. It can be seen that specimen type 4 has high tensile strength compared to remaining specimen types, and specimen type 2 has low tensile strength compared to 1,3 & 4.

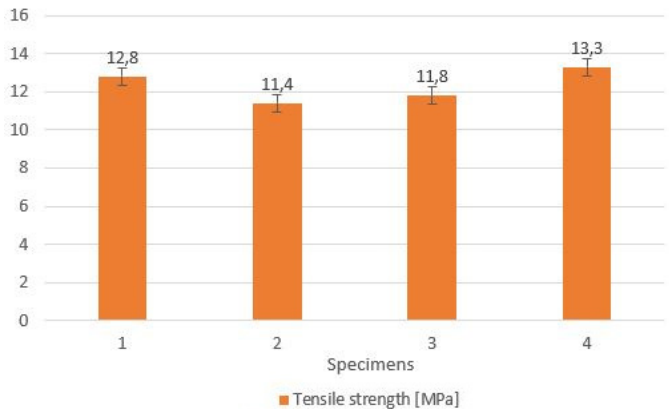


Figure 11: Average tensile strength.

Figure 12, when applying an equal amount of load to all specimens, specimen type 1 deflects high at low temperature compared to the remaining 3 specimen types, while specimen type 2 deflects less than that too at high temperature. Results are shown in Table 5.

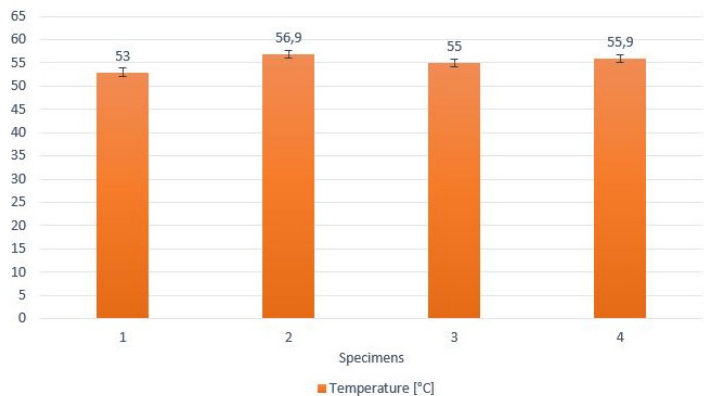


Figure 12: Average heat deflection temperature.

**Table 3:** Simulation results of three-point bending tests.

Specimen number	Side length [mm]	Wall thickness [mm]	$\sigma_1$ [MPa] at 0.05%	$\sigma_2$ [MPa] at 0.25%	Test results $E_r$ [MPa]	Simulation results $E$ [MPa]
1	2.4	0.6	0.625	3.12	545	1248.05
2	2.8	0.8	0.609	3.04	545	1217.30
3	3.2	1.0	0.598	2.99	651	1192.56
4	3.6	1.2	0.654	3.27	680	1308.80

**Table 4:** The results of tensile tests: strain at tensile strength  $\epsilon_M$ , nominal strain at tensile strength  $\epsilon_{IM}$ , nominal strain at break  $\epsilon_{IB}$ , tensile strength  $\sigma_M$ 

Specimen number	Side length [mm]	Wall thickness [mm]	$\sigma_{low}$ [MPa]	$\sigma_{high}$ [MPa]	$E_t$ [Mpa]	$\sigma_B$ [MPa]	$\epsilon_M$ [%]	$\epsilon_{IM}$ [%]	$\epsilon_B$ [%]	$\epsilon_{IB}$ [%]	$\sigma_M$ [MPa]
1	2.4	0.6	0.131	0.538	198	10.5	30	22	32	23	12.8
2	2.8	0.8	0.128	0.517	195	10.5	20	18	20	19	11.4
3	3.2	1.0	0.063	0.423	180	10.3	20	16	18	17	11.8
4	3.6	1.2	0.185	0.753	281	12.4	12	11	12	12	13.3

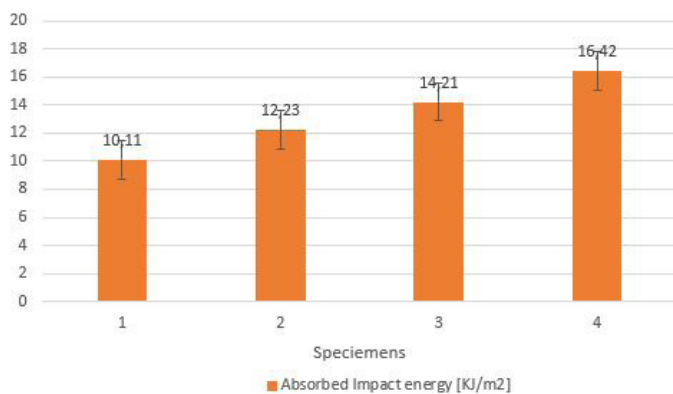
**Table 5:** The results of HDT tests.

Specimen number	Side length [mm]	Wall thickness [mm]	Average VST/HDT [°C]	Creep path [mm]	Load [g]	Scatter [°C]	Number of printed parts
1	2.4	0.6	53.0	0.46	306	0.80	3
2	2.8	0.8	56.9	0.25	306	1.90	3
3	3.2	1.0	55.0	0.25	306	0.30	3
4	3.6	1.2	55.8	0.21	306	0.60	3

The compression moduli ( $E_c$ ) results are shown in Table 6,  $E_c$  was high for specimen type 1 compared to remaining specimen types and specimen type 3 shows very less.

Flexural modulus is high for the 4<sup>th</sup> type specimen so it was stiffer compared to remaining specimen types and is shown in Table 7.

Figure 13, describes impact energy absorption and coefficient of variation. The energy absorption rate was in increasing order from specimen type one to four, while the coefficient of variation fluctuates. The results are shown in Table 8.

**Figure 13:** Average impact energy.

In tensile strength increasing the side length and wall thickness of honeycomb structure results gradual increase in tensile modulus. Specimen type 4 has a high tensile modulus (281 MPa).

For heat deflection temperature specimen type 2 resists maximum temperature (56.9°C) compared to other samples because the weight of specimen type 2 (2.0212 g) is greater than the remaining samples (1,2,3) with deflection of only about 0.25 mm. Specimen types 1 and 3 were deflected less compared to the deflections of specimen types 2 and 4, while deflections of specimen type 2 being the highest. This is because of the change in wall thickness and the width of the hexagonal cell.

Specimen type 1 has high compression modulus due to low surface area. As the surface area is increasing the compression modulus was varying because of the void space in the hexagonal cell increases.

The void space inside the cell structure is increasing from specimen type 1 to 4. So, the second specimen type has the highest deflection while the wall thickness compensated the side length in the case of specimen types 3 and 4.

Specimen type 4 possesses high flexural modulus so it is stiffer than compared to other specimens because of the wall thickness.

Specimen type 4 possesses the highest impact strength because of increasing wall thickness but less weight Compared to specimen type 2. The reason behind this is the increasing side length and wall thickness reduces the number of hexagonal cells. And the specimen type with less material and lightweight exhibits high strength. All specimens are between 10% to 80% of the hammer energy. When compared to previous literature they tested in different ways for different structures by changing fill density and only for the specific application.

**Table 6:** The results of compression test: compressive stress at 1% compressive strain  $\sigma_1$ , compressive yield strength  $\sigma_Y$ , yield compression  $\epsilon_Y$ , nominal yield compression  $\epsilon_{CY}$ , compressive strain at compressive strength  $\epsilon_M$ , nominal compressive strain at compressive strength  $\epsilon_{CM}$ .

Specimen number	$E_c$ [MPa]	$\sigma_1$ [MPa]	$\sigma_Y$ [MPa]	$\epsilon_Y$ [%]	$\epsilon_{CY}$ [%]	$\sigma_M$ [MPa]	$\epsilon_M$ [%]	$\epsilon_{CM}$ [%]	$\sigma_B$ [MPa]	Weight [g]	$\epsilon_B$ [%]
1	218	6.73	-	-	-	50	6.0	6.0	-	5.320	-
2	45.5	3.77	47.8	8.9	8.9	50	18.0	18.0	-	4.633	-
3	149	4.66	36.3	6.8	6.8	50	18.0	18.0	-	5.184	-
4	36.4	2.65	-	-	-	50	9.7	9.7	-	4.712	-

**Table 7:** The results of three-point bending test.

Specimen number	Side length [mm]	Wall thickness [mm]	$\sigma_{low}$ [MPa]	$\sigma_{high}$ [MPa]	$E_f$ [MPa]	$F_c$ [MPa]	Number of printed parts
1	2.4	0.6	0.37	1.46	545	14.6	5
2	2.8	0.8	0.37	1.47	545	14.7	5
3	3.2	1.0	0.57	1.82	651	19.2	5
4	3.6	1.2	0.13	1.53	680	17.6	5

**Table 8:** The results of Charpy test.

Specimen number	KJ/m	KJ/m <sup>2</sup>	Coefficient of variation [%]	Standard deviation [KJ/m <sup>2</sup> ]	Number of printed parts	Average weight [g]
1	0.040	10.11	10.82	1.095	5	1.678
2	0.048	12.23	10.67	1.306	5	2.021
3	0.056	14.21	9.073	1.288	5	1.678
4	0.065	16.24	12.19	2.002	5	1.892

Summarizing the discussion, it has been observed from the discussions for any compressive load-bearing conditions the specimen type 1 hexagonal cell dimensions can give the highest strength. For flexural, tensile and impact load-bearing conditions the specimen type 4 hexagonal cell dimension exhibits better properties and specimen type 2 hexagonal cell dimensions show good thermal properties.

## Conclusions

It has been observed that the number of hexagon cells decreases as the thickness and length of the hexagon cell increase. Void space and weight also has a significant effect on the properties of the printed product.

Analysis of the results suggests that the best hexagonal cell side length to thickness ratio is 3:1 to get ultimate tensile strength. This can be explained by if the cell thickness is other than one-third of the side length, the specimen easily breaks. So, to attain superior properties the cell thickness should be one-third of the side length.

It was observed that the weights of the specimen types 1 and 3 are nearly equal when the cell dimensions are increased.

It was proved that to get the optimum HDT properties hexagonal cell length to thickness ratio should be 3.5:1 because it consists of a high amount of material, which resist maximum temperature and deflection rate was also less.

To maintain appropriate void space and to get good compression properties the hexagonal cell length to thickness ratio should be 4:1 so that load can evenly distribute on the cells. Specimen type with 3:1 ratio compressed at low value due to more void space.

For the three-point bending test, the best ratio to exhibit good flexural properties is 3:1. Specimens with this ratio show great flexural strength because with the increase in cell dimensions load-bearing capability increases.

Specimens bear maximum load at 3.6:1.2, due to high wall thickness on load acting side. So, to attain maximum impact strength and low overall weight the hexagonal cell side length should be triple than wall thickness.

Solid parts can be replaced by hexagonal structures without compromising their strength, which is a benefit to the wide range of industrial applications. These structures are also suitable for pillars due to these structures have good impact strength and compression strength.

The glue which was applied to the print bed stucked to the bottom layer of the 3D printed samples. So, specimens should be washed after printing to make sure the results were dependable.

It was observed that there were holes formed on the top layer of the specimens because there was no support in the hollow part of the honeycomb. And the material was projected upward (convex shape) because of the pressure in the hollow part of the honeycomb. This can be overcome by increasing the thickness of the top layer but the thickness might affect the results.

## Future scope

The design example presented here would lead the future design engineers for low-cost composite fabrication. In this research, only hexagonal honeycomb is tested for compressive strength, tensile, bending, impact and HDT. In the future, other categories

of cellular structure such as truss and lattice structure could be investigated to determine the optimized properties. The build time and mechanical properties can be optimized, by changing the specimen orientation for printing.

### Acknowledgement

This research is supported by IKW and the University of Applied sciences Kaiserslautern. I would also like to thank Dr. Monis Kazmi for advising on the documentation and presentation.

### References

1. Syed MT, Elias PK, Amit B, et al. Additive manufacturing: scientific and technological challenges. Market uptake and opportunities. *Materials today*. 2017; 1: 1-16.
2. Holzmann P, Robert J, Aqeel Breiteneker A, et al. User entrepreneur business models in 3D printing. *Journal of Manufacturing Technology Management*. 2017; 1: 75-94.
3. Yuanbin W, Blache R, Xun X. Selection of additive manufacturing processes. *Rapid Prototyping Journal*. 2017; 2: 434-447.
4. Ventola CL. Medical Application for 3D Printing: Current and Projected Uses. *Medical Devices*. 2014; 10: 704-11.
5. Klahn C, Leutenecker B, Meboldt M. Design for Additive Manufacturing-Supporting the Substitution of Components in Series Products. *Procedia CIRP*. 2014; 138-143.
6. Ze-Xian L, Yen TC, Brian MR, et al. Perspective on 3D printing of separation membranes and comparison to related unconventional fabrication techniques. *Journal of Membrane Science*. 2017; 1: 596-613.
7. Jichang X, Haifei L, Jinzhong L, et al. Additive manufacturing of tungsten using directed energy deposition for potential nuclear fusion application. *Surface and Coatings Technology*. 2021; 409.
8. Shahrubudin N, Lee TC, Ramlan R. An overview on 3D printing technology. *Technological, Material and Applications*. *Procedia Manufacturing*. 2019; 1286-1296.
9. Silbernagel C. Additive Manufacturing 101-4: What is material jetting? *Canada Makers*. 2018.
10. Jonas W, Alexander G, Christian M. Laser powder bed fusion manufacturing of aluminium honeycomb structures. *International Journal of Mechanical Sciences*. 2020; 180.
11. Vijayavenkataraman S, Jerry YHF, Wen FL. 3D Printing and 3D Bio printing in Paediatrics. *Bioengineering*. 2017; 63: 1-11.
12. Low Z, Chua YT, Ray BM, et al. Perspective on 3D printing of separation membranes and comparison to related unconventional fabrication techniques. *Journal of Membrane Science*. 2017; 1: 596-613.
13. Yuanbin W, Robert B, Xun X. Selection of additive manufacturing processes. *Rapid Prototyping Journal*. 2017; 2: 434-447.
14. Cagri O, Ryan K, Mauro F, et al. Microstructure and mechanical properties of three dimensional-printed continuous fiber composites. *J. Compos. Mater.* 2019; 2: 271-280.
15. Daminabo SC, Goel S, Grammatikos SA, et al. Fused deposition modelling-based additive manufacturing (3Dprinting): Techniques for polymer material systems. *Materials Today Chemistry*. 2020; 100248.
16. Liu Z, Wang Y, Wu B, et al. A critical review of fused deposition modelling 3D printing technology in manufacturing polylactic acid parts. *International Journal of Advanced Manufacturing Technology*. 2019; 1-13.
17. Matsuzaki R, Ueda M, Namiki M, et al. Three-dimensional printing of continuous-fiber composites by in nozzle impregnation. *Scientific Reports*. 2016; 6: 23058.
18. Brennan-Craddock J, Brackett D, Wildman R, et al. The design of impact absorbing structures for additive manufacture. *Journal of Physics*. 2012; 382: 012042.
19. Bates SRG, Farrow IR, Trask RS. 3D Printed polyurethane honeycombs for repeated tailored energy absorption. *Materials and Design*. 2016; 172-183.
20. Abueidda DW, Bakir M, Al-Rub RKA, et al. Mechanical properties of 3D printed polymeric cellular materials with triply periodic minimal Surface architectures. *Materials and Design*. 2017; 255-267.
21. Chen Y, Li T, Jia Z, et al. 3D printed hierarchical honeycombs with shape integrity under large compressive deformations. *Materials and Design*. 2018; 226-234.
22. Chen L, Zhang J, Du B, et al. Dynamic crushing behaviour and energy absorption of graded lattice cylindrical structure under axial impact load. *Thin Walled Structures*. 2018; 333-343.
23. Harris JA, Winter RE, McShane GJ. Impact response of additively manufactured metallic hybrid lattice materials. *International Journal of Impact Engineering*. 2017; 177-191.
24. Li T, Chen Y, Hu X, et al. Exploiting negative Poisson's ratio to design 3Dprinted composites with enhanced mechanical properties. *Materials and Design*. 2018; 247-258.
25. Panda B, Leite M, Biswal BB, et al. Experimental and numerical modelling of mechanical properties of 3D printed honeycomb structures. *Measurement*. 2018; 495-506.
26. Lubombo C, Huneault MA. Effect of Infill Patterns on the Mechanical Performance of Lightweight 3D-Printed Cellular PLA Parts. *Materials Today Communications*. 2018; 241-228.
27. Sethu Ramalingam P, Mayandi K, Balasubramanina V, et al. Effect of 3D printing process parameters on the impact strength of onyx-Glass fiber reinforced composites. *Materials Today: Proceedings*. 2021; 7: 6154-6159.
28. Handrik M, Majko J, Barnik F, et al. comparing mechanical properties of composites structures on Onyx base with different density and shape of fill. *Transportation Research procedia*. 2019; 616-622.

- 
29. Yousuf Pasha S, Schuster J, Ram Chowdary T. Impact of 3D printing patterns and post-consolidation pressure on mechanical properties of FDM printed samples. *American Research Journal of Material Science*. 2021; 1: 1-10.
30. Miranda A, Leite M, Reis L, et al. Evaluation of the influence of design in the mechanical properties of honeycomb cores used in composite panels. *Journal of Materials. Design and Applications*. 2021; 6: 1325-1340.